Mechanical properties of membranes composed of gel-phase or fluid-phase phospholipids probed on liposomes by atomic force spectroscopy

Oumaima Et Thakafy, N. Delorme, Cedric Gaillard, Cristelle Mériadec, Franck Artzner, Christelle Lopez, Fanny Guyomarc'H

Mechanical properties of membranes composed of gel-phase or fluid-phase phospholipids probed on liposomes by atomic force spectroscopy

Oumaima ET-THAKAFY[‡], Nicolas DELORME[†], Cédric GAILLARD[‖], Cristelle MERIADEC[§], Franck ARTZNER[§], Christelle LOPEZ[‡], Fanny GUYOMARC'H[‡*]

[‡] STLO, INRA, Agrocampus Ouest, 35000, Rennes, France

[‖] UR BIA 1268 Biopolymères Interactions Assemblages, INRA, 44316 Nantes, France

[§]Institut de Physique de Rennes, UMR 6251, CNRS, Université de Rennes 1, 263 Av. Général Leclerc, 35042 Rennes, France

† UMR CNRS 6283 Institut des Molécules et Matériaux du Mans, Université du Maine, Université Bretagne-Loire, 72000 Le Mans, France

[*]Corresponding author: Fanny Guyomarc'h

Key words: small unilamellar vesicle; Phase state; Bending modulus; Young's modulus; Atomic force microscopy

Abstract

In many liposome applications, the nanomechanical properties of the membrane envelope are essential to ensure e.g. physical stability, protection or penetration into tissues. Of all factors, the lipid composition and its phase behavior are susceptible to tune the mechanical properties of membranes. To investigate this, small unilamellar vesicles (SUV; diameter <200 nm),

referred to as liposomes, were produced using either the unsaturated 1,2-dioleoyl-sn-glycero-3-phosphocholine (DOPC) or the saturated 1,2-dipalmitoyl-sn-glycero-3-phosphocholine (DPPC) in aqueous buffer at pH 6.7. The respective melting temperatures of these phospholipids were -20°C and 41°C. X-ray diffraction analysis confirmed that at 20°C DOPC was in the fluid phase and DPPC was in the gel phase. After adsorption of the liposomes onto flat silicon substrates, atomic force microscopy (AFM) was used to image and probe the mechanical properties of the liposome membrane. The resulting force-distance curves were treated using an analytical model based on the shell theory to yield the Young's modulus (E) and the bending rigidity (k_C) of the curved membranes. The mechanical investigation showed that DPPC membranes were much stiffer (E = 116 ± 45 MPa) than those of DOPC (E = 13 ± 9 MPa) at 20°C. The study demonstrates that the employed methodology allows discrimination of the respective properties of gel- or fluid-phase membranes when in the shape of liposomes. It opens perspectives to map the mechanical properties of liposomes containing both fluid and gel phases or of biological systems.

I. INTRODUCTION

In the recent years, small unilamellar vesicles of phospholipids (< μm diameter) have gained increasing interest in various liposome technologies, e.g. as drug delivery systems in pharmacy or as protective cargo capsules for cosmetics, nutraceuticals or for food design[1,2]. They are also interesting models to investigate and possibly control *in vivo* biological signaling mechanisms involving extracellular vesicles such as the so-called exosomes[3,4]. The

composition of the phospholipids, i.e. the acyl chains' saturation/unsaturation and length, impacts their phase state in the liposomes at ambient temperatures[5]. This, in turn, is likely to affect the mechanical properties of the liposomes, which are of paramount importance for these applications. Mechanical properties direct the stability, size, shape and fusion of the liposomes [6–8]as well as the membrane fluidity/rigidity or permeability and hence their loading capacity or their ability to penetrate tissues[9–13]. For example, the permeability of various saturated polar lipid membranes to glucose strongly increases as the lipid undergoes gel-to-liquid disordered (l_d) phase transition[14]. As another example, milk sphingomyelin exhibited maximum permeability at temperatures where gel-to-l_d phase transition occurs[13]. This has important consequences on the formulation and design of liposomes, as the desirable mechanical properties will differ depending on the application and temperature, e.g. storage at ambient temperature, transdermal delivery of drugs, etc. Experimental techniques to measure the mechanical properties of liposomes, such as the pipette aspiration technique, osmotic or mechanical compression, shear-induced or optical tweezers deformation[7]are often designed for large objects of the μm length scale. For liposomes at the nanoscale, such as small unilamellar vesicles, indentation measurement using atomic force microscopy (AFM) has proven a valuable and sensitive approach[15–20]. The liposomes, adsorbed onto a flat substrate, are indented by the AFM with low penetration distances (i.e. the order of magnitude of the membrane thickness) and at as low force values as down to the pN. The major advantage of AFM over a nano-indenter is also its imaging capacity, which allows to locate liposomes and

to indent them centrally, even though not perfectly normally[16]. In a pioneering study, Laney et al.[17] extracted synaptic liposomes (~110 nm diameter) from the electric organ of the electric ray *Torpedo californica*, immobilized them by adsorption onto mica and measured elastic moduli values in the range 0.2 – 1.3 MPa. Liang et al.[19,2119,22] followed the same approach on small (40-160 nm) liposomes of egg phosphadidylcholine (mainly stearoyloleoylphosphatidylcholine, SOPC) and found that the elastic modulus increased with the addition of up to 50 mol % cholesterol from ~2 to 13 MPa. However, these authors used an adaptation of the Hertz model for their calculations that assumed the liposomes to be homogeneous filled spheres. By implementing the shell deformation theory, Delorme and Fery[16] obtained higher elasticity values of ~110 MPa by indenting DPPC (dipalmitoylphophastidylcholine) and proposed that the Hertz model underestimated the mechanical properties of the liposomes. However, due to its mono-unsaturation, egg PC has a melting temperature (Tm) of -15°C and is therefore in the l_d or liquid crystalline (Lα) phase at 20°C, while the fully saturated DPPC is in the gel or solid-ordered (s_o) phase (Tm = 41.7°C)[22,23]. Therefore, it is yet to assess whether the AFM indentation measurement combined with the shell theory interpretation is sensitive enough to discriminate liposomes with presumably different mechanical properties of their membranes, e.g. by comparing saturated and unsaturated phospholipids in different physical phases at 20°C.

When the membranes are spread as two-dimensional supported lipid bilayers (SLBs), measurement of the rupture force of membranes using AFM indentation has proven to fully

resolve mechanical differences between phospholipids with various chain lengths, saturation degrees or head groups[24]. However, calculation of the SLBs' effective elasticity using indentation of the membrane and the Hertz model requires careful and narrow experimental conditions not to be affected by the support[25] Furthermore, direct measurement on small liposomes would encompass possible curvature effects. Indeed, their high membrane curvature may affect their mechanical properties, as lateral intermolecular distances and forces vary across the bilayer's thickness[26,27]. However, indentation measurements on 3D vesicles may be either impossible [28], require high deformation of the objects[19] or somewhat depend on the composition of the internal medium, if different from the surrounding medium[29]. For these reasons, there is interest to assess indentation measurement of the mechanical properties of membranes directly on volumetric objects such as liposomes.

In the present study, the respective elasticities and bending rigidities of membranes of either the unsaturated phospholipid dioleoylphosphatidylcholine (DOPC) or the saturated phospholipid dipalmitoylphosphatidylcholine (DPPC) as shaped in the form of liposomes, were measured at 20°C using AFM indentation and the shell theory. The results were discussed in light of the respective phase states of the two phospholipids at 20°C and showed that AFM indentation is a sensitive method to assess the mechanical properties of 3D membrane objects at the nanoscale.

II. EXPERIMENTAL METHODS

2.1. Materials

Pure phospholipids 1,2-dioleoyl-sn-glycero-3-phosphocholine (DOPC; 18:1; >99%) and 1,2-dipalmitoyl-sn-glycero-3-phospholcholine (DPPC; 16:0; >99%) were purchased from Avanti Polar Lipids (Alabaster, AL). PIPES (1,4-piperazinediethanesulfonic acid) buffer was prepared as: PIPES 10 mM (purity ≥99%; Sigma-Aldrich, Milwaukee, WI, USA), NaCl 50 mM (Sigma), and $CaCl_2$ 10 mM (Sigma) were dissolved in Milli-Q water and adjusted to pH 6.7 using NaOH 5 M.

2.2. Preparation of liposomes

Samples were prepared by dissolving appropriate quantity of the lipid powder of DOPC or DPPC in glass vials with chloroform/methanol (4:1 v/v). The organic solvent was then evaporated at 40 °C under a stream of dry nitrogen. The dried lipid films were hydrated with PIPES-NaCl-$CaCl_2$ buffer at 70°C to reach a final concentration of 0.1 wt. % lipids then thoroughly vortexed. Small unilamellar vesicles (SUV) were produced at 65°C by sonication using a Q700 equipment (Q-sonica, Newtown, CT, USA) and a microtip operating at 50% amplitude (~400 W) for 30 min. After sonication, the SUV suspension was left to cool and equilibrate at room temperature (20°C). The SUV produced according to this protocol will be designated as "liposomes" throughout this report.

2.3. Dynamic light scattering (DLS)

The size distribution and the average hydrodynamic diameter (D_h) of the vesicles were measured in PIPES-NaCl-$CaCl_2$ buffer at 20°C by dynamic light scattering (DLS) on a

Zetasizer Nano ZS (Malvern Instruments, Worcestershire, United Kingdom). Measurements were carried out at a scattering angle of 173° and a wavelength of 633 nm. The average D_h (± 5 nm) was calculated from the intensity distribution using conversion into an autocorrelation function which is then analyzed with the Stokes-Einstein relation, assuming that particles had a spherical shape. The viscosity of the solution was 1.003 mPa.s at 20°C and the refractive index of the solvent was 1.33.

2.4. Differential scanning calorimetry (DSC)

The thermotropic properties of DOPC or DPPC were measured on multilamellar vesicles using a differential scanning calorimetry (DSC) Q1000 apparatus (TA Instruments, Newcastle, USA). Multilamellar vesicles (MLV) were produced by rehydration of the lipid films with PIPES-NaCl-$CaCl_2$ buffer at 65°C to reach a final concentration of 20 wt. % lipids, then thorough vortex mixing. MLV are preferred over unilamellar vesicles in order to accommodate the high bilayer concentration. They also allow higher resolution of the DSC thermograms thanks to higher cooperativity of the molecules[30] . The samples were introduced in 20 µL aluminum pans that were then hermetically sealed. An empty pan was used as a reference. The samples were heated at 2°C.min^{-1} from - 40°C to 70°C. The calibration of the calorimeter was performed with indium standard (melting point = 156.66°C, ΔH melting = 28.41 J.g^{-1}). The thermal measurements were performed in triplicate. Standard parameters were calculated by the TA software (Universal Analysis 2000, v 4.1 D).

2.5. Temperature-controlled X-ray diffraction (XRD)

X-ray scattering experiments were performed on the home-made Guinier beamline at IPR[31] . A two-dimensional Pilatus detector with sample to detector distance of 232 mm allowed the recording of XRD patterns in the range 0.013 $Å^{-1}$ to 1.742 $Å^{-1}$, thus covering both the small and wide-angles regions of interest to characterize the lamellar structures and to identify the packing of the acyl chains, respectively. Diffraction patterns displayed series of concentric rings as a function of the radial scattering vector $q = 4 \pi \sin\theta / \lambda$, where 2θ is the scattering angle and $\lambda = 1.541Å$ is the wavelength of the incident beam. The channel to scattering vector q calibration of the detector was carried out with silver behenate[32]. Small volumes (around 10 µL) of samples containing DOPC or DPPC vesicles were loaded in thin quartz capillaries of 1.5 mm diameter (GLAS W. Muller, Berlin, Germany) and inserted in the set-up at a controlled temperature.

2.6. Transmission electron microscopy (TEM)

The observation of DOPC and DPPC Liposomes by cryo-TEM was realized as described in previous work[33]. The samples were prepared using a cryoplunge cryo-fixation device (Gatan, Pleasanton, CA, USA) in which a drop of the aqueous suspension was deposited on to glow-discharged holey-type carbon-coated grids (Ted Pella Inc., Redding, CA, USA). The TEM grid was then prepared by blotting the drop containing the specimen to a thin liquid layer remained across the holes in the support carbon film. The liquid film was vitrified by rapidly plunging the grid into liquid ethane cooled by liquid nitrogen. The vitrified suspension of liposomes was mounted in a Gatan 910 specimen holder that was inserted in the microscope

using a CT-3500-cryotransfer system (Gatan, USA) and cooled with liquid nitrogen. TEM images were then obtained from liposomes suspension preserved in vitreous ice and suspended across a hole in the supporting carbon substrate. The samples were observed under low dose conditions (< 10 $e^-.A^2$), at -178 °C, using a JEM 1230 'Cryo' microscope (Jeol, Japan) operated at 80 keV and equipped with a LaB6 filament. All the micrographs were recorded on a Gatan 1,35 K × 1,04 K × 12 bit ES500W CCD camera.

2.7. Atomic force microscopy (AFM)

2.7.1. Indentation of liposomes

Simple open liquid sample cells were fabricated by gluing small (~0.5 × 1 cm^2) pieces of silicon substrate (molecular orientation 100) onto diagnostic glass slides (Thermo Scientific, Waltham, MA, USA). After thorough cleaning of the cell with ethanol, water and UV/O_3, the liposome suspension equilibrated at 20°C was deposited onto the clean silicon surface then left to incubate at 20°C for 30 min. The droplet was then gently exchanged with PIPES-NaCl-$CaCl_2$ buffer at 20°C to remove the un-adsorbed liposomes. The sample was then imaged in contact mode using an MFP-3D Bio AFM (Asylum Research, Santa Barbara, CA, USA), with a typical scan rate of 1 Hz for 20 × 20 μm^2 and 256 × 256 pixels images, silicon MLCT probes (nominal spring constant k ~0.03 $N.m^{-1}$ – Bruker Nano Surfaces, Santa Barbara, CA, USA) calibrated extemporaneously using the thermal noise method, and loading forces typically below 1 nN. Upon adsorption onto the flat surface, the spherical liposomes deform into spherical cap geometry. AFM imaging of large area (typical size) allows localization of

the adsorbed liposomes, then closer images (typically 2 × 2 μm^2 or less) were recorded and sections were drawn across the images in order to measure the individual liposome's height (H) and base width (W). The AFM probe was then positioned above the center of each liposome and individual force curves (n > 60) were recorded with a set point of 200 pN, a distance of 100 nm and a Z-piezo speed of 2 $\mu m.s^{-1}$. In these conditions, indentation of the AFM tip into the liposome did not exceed ~5 nm, thereby allowing measurement of the mechanical properties in the elastic regime of the membrane. The approach curves were then treated using the shell theory as described in the result section.

For data visualization and analysis, Gwyddion 2.47 software was also used, as a means to deduce the local radius of curvature (R_c) at the top of individual adsorbed liposomes over a distance of ~130 nm both sides of the apex (130 nm being the estimated radius of the membrane area affected by indentation by a 20-nm radius MLCT probe). The R_c values of individual liposomes were input in the calculation of the Young modulus (see below). Measurement of the local R_c values at the apex of individual liposomes, instead of for the complete objects, avoided errors due to imperfect (e.g. flattened) spherical cap geometry of the liposome upon adsorption, and/or errors due to convolution by the AFM tip. The latter may indeed overestimate lateral dimensions of the liposomes by as much as the tip diameter, but can be avoided as long as near-normal contact is maintained between the tip and the liposomes, which is the case when measuring R_c at their apex.

2.7.2. Measurement of the bilayer thickness

Immediately after sonication at 65°C, 10 µg of the hot lipid suspension were deposited onto freshly cleaved mica in an Asylum Research open liquid cell, then incubated at 65°C for 60 min. Slow cooling of the samples was performed using a programmed incubator as in Murthy et al.[34] to yield supported lipid bilayers (SLB). Once equilibrated at 20°C, the bilayers were extensively rinsed and exchanged with PIPES-NaCl-$CaCl_2$ buffer. AFM imaging of the bilayers was then performed in the same buffer and in contact mode using MSNL probe (nominal spring constant k ~0.03 $N.m^{-1}$ – Bruker Nano Surfaces, Santa Barbara, CA, USA) with the same imaging parameters already cited. The probes were calibrated extemporaneously using the thermal noise method. Force spectroscopy curves were then acquired at 20°C by using force-volume imaging of the bilayers (typically 10 × 10 μm^2 or less) with a typical set point of 20 nN and a piezo speed of 2$\mu m.s^{-1}$.

2.8. Statistical analysis

The results are presented as mean value ± standard deviation. Analysis of variance was performed using the General Linear Model procedure of Statgraphics Plus version 5 (Statistical Graphics Corp., Englewood Cliffs, NJ). Differences were significant for $p < 0.05$.

III. RESULTS AND DISCUSSION

3.1. Phase state of DOPC and DPPC at 20°C

The thermal phase behavior of unsaturated (18:1) DOPC and saturated (16:0) DPPC phospholipids (chemical structures shown in Fig1.A) was examined using DSC and the

results were correlated with the structural analysis performed by XRD. Fig1.B shows the respective DSC heating thermograms of both lipids in the same conditions. For DOPC, the thermogram shows a very low temperature of L_β to L_α (gel to fluid) phase transition at T_m = -20°C, in good agreement with previous reports [11,35,36]. Meanwhile, the heating of DPPC revealed two endotherms, characteristic of the L_β (gel) to $P_{\beta'}$ (ripple) transition at T_m = 37.09 °C and of the $P_{\beta'}$ (ripple) to L_α (fluid) transition at T_m= 41.01°C, also in good agreement with previous reports [34,35,37] . XRD experiments allowed identification of the lipid phases at 20°C (Fig. 1C). For this, the MLV are interesting not only to investigate the lateral packing of the acyl chains (at large q), but also to confirm the lamellar organization of the phospholipid (at small q). For DOPC, the absence of diffraction peak at wide angles and a lamellar organization characterized at small angles, confirmed the L_α phase of DOPC at 20°C. DPPC multilamellar vesicles exhibited a single broad peak at q~1.5 $Å^{-1}$ corresponding to the formation of ordered phase packed in pseudo-hexagonal lattice and a lamellar organization at small angles, showing the formation of a $L_{\beta'}$ organization of DPPC at 20°C. The tilt of the acyl chains may have been induced by the multilamellar organization of the DPPC molecules in the vesicles. Since AFM experiments on DPPC molecules were performed in SUV, the ordered phase state of DPPC molecules in SUV at 20°C was also proved by XRD experiments performed on SUV of DPPC. As previously reported in literature[38], the high curvature of expected SUV of DPPC do not allow the recording of a peak at wide angles. Nevertheless, the Small Angles X-ray Scattering could be performed upon heating of the

SUV. Both high and low temperature spectra can be fitted as an individual membrane using equation (1):

$$I(q) = \frac{1}{q^2}\left[\frac{\sin(q.e_{HG}/2)}{q.e_{HG}}.e^{-(q.r)^2} + \frac{\sin(q.e_{CH2}/2)}{q.e_{CH2}}\right]^2 \quad (1)$$

with e_{HG}, the headgroup thickness, e_{CH2}, the aliphatic chain thickness and r the rugosity of the headgroup/water interface.

The full analysis demonstrates a contraction of 2Å of both e_{HG} and e_{CH2} at the gel-fluid transition at 40-44°C (Fig. 1D). This showed that the DPPC molecules in SUV are sensitive to temperature and consequently in the gel phase at room temperature. In conclusion, DSC and XRD confirmed that DOPC (unsaturated; Tm = -20°C) and DPPC (saturated; Tm = 41°C) were respectively present in fluid and gel phases at 20°C.

3.2. Morphology of the liposomes at 20°C

Electron microscopy, dynamic light scattering (DLS) and AFM imaging were used to characterize the morphology (size and shape) of the liposomes obtained after sonication (Fig 2). Cryo-TEM images showed that DOPC and DPPC vesicles were essentially unilamellar and spherically shaped. However, while DOPC liposomes consistently exhibited circular cross-sections (Fig 2A), DPPC could show both rounded and/or somewhat faceted membranes (Fig 2D). The presence of angle facets was attributed to the physical gel state of DPPC at 20°C[39]. Cryo-TEM images revealed variable liposome diameters (from tens to

hundreds of nm) which corresponded to the size distribution measured by DLS (Fig 2B, E). For DOPC, the size distribution was monomodal with a mean diameter D_h at 120 ± 69 nm (Fig 2.B). Whereas, DPPC liposomes exhibited a shouldered size distribution with a mean diameter D_h of 132 ± 73 nm for the whole distribution (Fig 2.E; Table1).

In the next step, the liposomes were immobilized by adsorption onto silicon to be first imaged then indented using an AFM probe. Images recorded in contact mode showed that DOPC and DPPC liposomes were perfectly stable on the flat substrate. However, it was not possible to prevent non-destructive deformation due to adsorption, as previously reported[19,40]. The AFM images were also used to measure the height *H* and basal width *W* of adsorbed individual liposomes in order to prove that objects observed in AFM images corresponded truly to liposomes. To do this, the adsorbed liposomes were considered to adopt a spherical cap geometry and their volume was calculated as:

$$V = \frac{\pi H}{6}\left(\frac{3}{4}W^2 + H^2\right) \quad (2)$$

From (Eq.2), the mean diameter of a sphere of equivalent volume was inferred and compared with DLS data (Table 1; Figures 2B and E). The mean diameter values were of similar orders of magnitude in both methods; and whatever the method used, DOPC liposomes always exhibited smaller diameters than DPPC ones. This confirmed that the adsorbed objects visible on the AFM images truly were liposomes. However, the mean diameter results measured by AFM were higher than DLS probably because larger liposomes were preferably chosen out of

large-area images (such as shown on Figure 2) to perform close-up views and indentation measurements (Table1).

3.3. Mechanical properties of liposomes as a function of phase state at 20°C

3.3.1. Bilayer thickness

The average bilayer thickness d was measured in the conditions used in this work: temperature 20°C, pH=6.7, 50 mM NaCl and 10 mM $CaCl_2$. This measurement was performed using atomic force spectroscopy on SLB of DOPC or DPPC spread onto freshly cleaved mica. Average values of d were obtained from measurements performed on various regions of different samples (n=50). In a typical force spectroscopy experiment, the AFM tip approaches the surface until a mechanical contact with the SLB is established. Then, the bilayer is elastically deformed by the AFM probe until the tip ruptures (breaks through) the membrane, thereby coming into contact with the substrate. The indentation *vs* force curves exhibited breakthrough events[23,34,41] where the jump-through distance (noted d) was assimilated as the bilayer's thickness[34]. The limitations of this measurement were discussed elsewhere[42] and efforts were taken to regard bilayer compression. Fig.3A and C show three examples of force-distance curves for each type of lipid bilayer. The d mean values obtained were 3.91 ± 0.46 nm, and 4.93 ± 0.47 nm for DOPC and DPPC bilayers, respectively. This thickness difference between fluid and gel phases was perfectly detected by AFM spectroscopy, in agreement with previous works[25,43]. In the literature, Nagles and Tristram-Nagles[44] also determined the thicknesses of DOPC and DPPC fully hydrated bilayers using

XRD and obtained a value of 3.6 nm for DOPC in the fluid phase and of 4.4 nm for DPPC in the gel phase. It should be noted that DOPC has two unsaturated 18 hydrocarbon chains and DPPC has two fully saturated 16 hydrocarbon chains (Fig1A). Unsaturation is the main reason that adversely affected chain elongation and molecular packing[45], making DPPC bilayers more ordered and thicker than DOPC bilayers at room temperature.

Noteworthy, the value of the force at which the SLB ruptured (i.e., the breakthrough force) was higher for DPPC (2-3 nN) than for DOPC (<1 nN), in agreement with their respective phase states [46–48]. The lower absolute values found in the present study may be accounted for the lower ionic strength and the sharper AFM tip (radius of MNSL tip ~2 nm) in comparison to previous works.

3.3.2. Mechanical properties of DOPC or DPPC liposomes:

In this work, we show that AFM spectroscopy could be used to discriminate and compare the mechanical properties of very small liposomes (~150 nm) in different phase states. Calculations of the Young modulus E and bending modulus k_C, based on the shell theory model, were done on DOPC or DPPC liposomes respectively in fluid or gel phase. In order to limit the plastic deformation, force distance curves were recorded over 100 nm distance with a set point of 200 pN maximal force. Typical examples are shown in Fig. 3 B and D. In these conditions, the approaching and retracting curves were superimposed, demonstrating the elastic behavior of the membrane (not shown). The tip-membrane contact was defined as the point where significant positive slope appeared. According to the shell theory developed by

Reissner [49] then Fery et al. [16,50], the Young modulus E of thin-shelled spherical micro-capsule under a point load scales with the bilayer's stiffness, k, which was deduced from the slope of the linear region of each force curve after the tip-membrane contact, i.e. in the small deformation region (Fig 3.B and D). As k strongly depends on the size of the individual liposomes[21], it has to be normalized by the local radius of curvature R_c of the individual liposomes[16] to describe their mechanical properties. Calculation of E requires the bilayers' stiffness k, the local radius of curvature R_c (see section 2.7.1), the bilayer's thickness d (Table1) and the Poisson ratio ν, taken as 0.5:

$$E = \frac{1}{C}\,\frac{kR_C\sqrt{3(1-\nu^2)}}{4\mathrm{d}^2} \qquad (3)$$

In equation 3, C is a coefficient that accounts for the double deformation of an adsorbed shell object, such as liposomes, upon indentation by the AFM tip. Indeed, whereas membrane deformation occurs at the contact point between the tip and the liposome, simultaneous deformation also occurs at the contact area between the liposome and the substrate[51]. In their recent paper, Bery et al.[52] produced calculations for a correction factor, C, to be applied as a function of the relative radii of the tip (20 nm) and liposome, and of the shell thickness relative to the radius of the liposomes (Table 1). Since that dimensions were similar for both the DOPC and DPPC liposomes, C was ~ 0.55 for both types of liposomes.

In another way, the mechanical properties of liposomes can be also represented by the bending rigidity k_C, which is expressed in terms of the same parameters and is also common in the literature:

$$k_C = \frac{E\mathrm{d}^3}{12(1-\nu^2)} \qquad (4)$$

Calculation of the Young's modulus, regardless of liposome size, showed that the DPPC liposome membranes (L_β) E= 116 ±45 MPa were significantly more elastic at 20°C than DOPC liposome membranes (L_α) which exhibited a lower value of E = 13 ± 9 MPa (Fig.4.A and B; $p < 0.05$). Accordingly, the liposome membranes composed of DPPC were also stiffer with k_C = (15.5 ± 6) $\times 10^{-19}$J (360 k_BT) than those composed of DOPC with k_C = (0.9 ± 0.6) $\times 10^{-19}$J (22 k_BT) (Fig.4.C and D; $p < 0.05$). To verify that electrostatic repulsion was not implicated in the force curves near the contact point, we compared the results acquired on DPPC liposomes with varying surface charge, taken as the zeta potential and measured as described in Makino et al.[53]. The DPPC liposomes were positively charged with a zeta potential of 18 mV in PIPES buffer (ionic strength I=0.09); and barely charged with a zeta potential of 0.11 mV in PBS buffer (14 mM KH_2PO_4, 200 mM Na_2HPO_4, NaCl 1.36 M, KCl 20 mM; I=1.99; pH= 7.2). The Young's modulus showed a mean value of E= 120 ± 39 MPa in PBS buffer and no significant difference was found between the Young moduli values obtained in the two buffers ($p > 0.05$). This result showed that force measurement of DPPC membrane was not influenced by electrostatic interaction between the AFM probe and the liposomes.

The Young modulus was also estimated using the R_c of the whole liposome, which involves the two parameters H and W (equation A.1). The results showed that the elasticity of DPPC

was higher (183 MPa) than that obtained by local R_c (116 MPa), whereas E was not significantly changed for DOPC. With either methods of R_c calculation, the results therefore showed that AFM indentation was able to detect significant differences in the elasticities of the two membranes depending on their fluid or gel phase state. However, the quantification of the mechanical properties was found very sensitive to calculation of R_c and to the liposome geometry. For these reasons, we chose to compare the liposomes using the method based on the local R_c using Gwyddion in order to avoid any effect due to the form adopted by the liposomes upon adsorption.

In conclusion, the structural differences between the fluid-phase DOPC and gel-phase DPPC bilayers as evidenced by DSC and XRD, induced by the unsaturation of the acyl chains (Fig1), resulted in significant difference in their respective mechanical responses. Hence, AFM force spectroscopy proved a sensitive method to compare the mechanical properties of small liposomes with different lipid compositions and phase states. Only few reports exist that have evaluated these mechanical parameters for similar systems of lipid membrane in 3D, especially for DOPC or DPPC using AFM spectroscopy (Table 2). Of all these studies, only Liang et al.[21] used AFM spectroscopy comparatively, on liposomes with increasing addition of cholesterol. Liang et al.[21] obtained Young's modulus of 1.97 ± 0.75 MPa, for liposomes in the fluid phase composed of egg PC (mixture of saturated and unsaturated polar lipids; mostly in the form of SOPC – stearoyl-oleoyl-phosphatidylcholine). Using an optical method, Meleard et al.[54] and Duwe et al.[55] respectively obtained bending rigidities of 1.27 ± 0.09 $\times 10^{-}$

^{19}J (31 k_BT) or 1.15 $\times 10^{-19}$J (28 k_BT) for liposomes composed of the saturated polar lipid DMPC (1,2-dimyristoyl-sn-glycero-3-phosphocholine) in fluid phase at 40°C (Tm = 24°C). Rawicz et al.[45] found values of ~0.9 × 10^{-19} J for bilayers of various synthetic 18:1 phospholipids. Another group, Hantz et al.[56] used the osmotic swelling method and found values of the Young's modulus of 15 MPa for DOPC liposomes in the fluid phase at 20°C. Delorme and Fery[16] obtained Young's moduli values of 110 ± 15 MPa for DPPC liposomes in the gel phase. Taking only account of the phase state conditions, the values available in the literature (Table 2) are in the same order of magnitude in comparison to the results showed in this work. Differences between studies could be attributed mainly to the nature of the lipids (carbon chain length, number of unsaturation), the temperature, the chosen technique or, for indentation studies, the mathematical model chosen for the calculation of R_c or E [57,58]. The presented results show that AFM indentation of liposome is a sensible method for comparison between different lipid membranes.

For the sake of comparison with the SUV (tridimensional organization), the elasticity of DPPC or DOPC membranes was calculated on the SLB (two dimensional organization) using AFM load curves performed in the same conditions as for the breakthrough force measurement. Only a larger MLCT probe was used for better sensibility. By attempting the fit of equation (5), the Young's moduli (noted E_{SLB}) and bending modulus (noted k_{C-SLB}) were calculated using the classical Hertz model:

$$F = \frac{4E_{SLB}\sqrt{R_{tip}}\,\delta^{\frac{3}{2}}}{3(1-\nu^2)} \quad \text{or } E_{SLB} = \frac{3}{4}\frac{k(1-\nu^2)}{\sqrt{R_{tip}\delta}} \qquad (5)$$

For which corresponds a bending modulus:

$$k_{C-SLB} = \frac{E_{SLB}\,\delta^3}{24\,(1-\nu^2)} \qquad (6)$$

Where the parameters are the same already cited for liposome membranes. In these equations, δ is the indentation distance and R_{tip} is the nominal radius of AFM MLCT tip (~20 nm).

The use of contact mechanics using the Hertz model on SLB is limited by the effect of confinement of the sample between the tip and the underlying substrate[59,60]. Furthermore, lipid bilayers are not anisotropic materials. However, previous investigations suggested that this calculation yet has comparative interest[25,61]. On SLBs, the Young modulus (E) of DOPC was found to be 27 ± 8 MPa with a corresponding bending modulus k_C= (0.88 ± 0.25) ×10^{-19}J, while the E and k_C of DPPC were found to be 31 ± 12 MPa and (2.03 ± 0.79) ×10^{-19}J, respectively. Therefore, the E and k_C parameters of DPPC and DOPC were less distinct when measured on SLB than on SUV (Table 2). Meanwhile, more dispersed E values were reported in the literature for SLBs than for liposomes, thereby indicating the higher sensitivity of this measurement upon experimental conditions in the case of SLB[25,61,62] (Table 2). To conclude, it is showed that membranes in the gel phase were more elastic and stiffer than the membranes in fluid phase regardless the lipid organization (2D or 3D). However, the values of E and k_C were more robust when measured on liposomes than on SLBs, where the presence

of the solid support affected the results depending on the indentation distance[25]. These comparisons show that liposomes are adequate systems to determine the elastic properties of lipid membranes. On the other hand, measurement of the breakthrough force is relevant for SLBs.

The structure of molecules and the intermolecular interactions that lead lipid molecules to self-assembly in bilayers, have a significant impact on the rigidity of these bilayers[63,64]. The elasticity of the membrane allows it to accommodate strain without failure, which is essential in many applications where the membrane need to resist shear stress, e.g. in transdermal application, in blood vessels, the epithelial cells of the gastrointestinal tract, etc. The hydrophobic interactions between the lipid molecules, in particular Van der Vaal interactions, are the major responsible of the fluidity and the rigidity of the membrane. The double bond in cis conformation interferes with hydrocarbon chain packing and destroys the cooperativity of the chain interactions in the bilayer[65,66] .

The presence of this double bonds reduces the hydrophobic interactions by increasing the distance between the hydrophobic moieties which decreases the stiffness of membrane[45].

IV. CONCLUSION:

The nano-indentation of DOPC and DPPC liposomes by AFM probe at low force load was able to provide local and discriminant information on the elastic properties of bilayer membranes in 3D organization without plastic deformation. The Young's moduli E and bending rigidity values k_C of gel phase DPPC membranes is significantly higher than that of

fluid phase DOPC ones at 20°C, in agreement with their different phase state. The perspective of this work is to investigate the mechanical properties of biological membranes with complex chemical composition and fluid/gel phase coexistence. Thanks to the high lateral resolution of AFM, it is expected that phase separation and correlated nanomechanical contrast may be measured directly on model liposomes or even biological vesicles.

V. ACKNOWLEDGMENTS

The Asylum Research MFP3D-BIO atomic force microscope was funded by the European Union (FEDER), the French Ministry of Education and Research, INRA, Conseil Général 35 and Rennes Métropole. The doctoral fellowship of author Et-Thakafy was funded by INRA CEPIA and Région Bretagne under the grant ARED 8806.

VI. APPENDIX:

The Young modulus values were also obtained using radius of curvature R_C of the whole individual liposomes. It was calculated using H and W of the individual liposomes[67], as:

$$R_C = \frac{0.25W^2 + H^2}{2H} \qquad (A.1)$$

The mechanical data obtained from literature were expressed either as the Young modulus E, the bending rigidity k_C or both. To complete and compare literature information in table 2; we used the following equations to provide both parameters for each cited reference:

For liposome (shell model):

$$k_C = \frac{E\mathrm{d}^3}{12(1-\nu^2)} \quad \Rightarrow \quad E = \frac{12(1-\nu^2)k_C}{\mathrm{d}^3} = \frac{9k_C}{\mathrm{d}^3} \quad (A.2)$$

For supported lipid bilayer (Hertz model):

$$k_{C-SLB} = \frac{E_{SLB}\,\mathrm{d}^3}{24\,(1-\nu^2)} \quad \Rightarrow \quad E_{SLB} = \frac{24\,(1-\nu^2)\,k_{C-SLB}}{\mathrm{d}^3} = \frac{18\,k_{C-SLB}}{\mathrm{d}^3} \quad (A.3)$$

E: Young modulus

k_C: bending rigidity

ν: Poisson coefficient (0.5)

d: membrane thickness

For the publication where the membrane thickness not shown, the following values were used to calculate the elasticity or the bending rigidity:

d(DMPC)= 3.6 nm [44]

d(DOPC) = 3.9 nm (present work)

REFERENCES

(1) Lasic, D. D. Novel Applications of Liposomes. *Trends Biotechnol.* **1998**, *16*, 307–321.

(2) Liu, W.; Ye, A.; Liu, C.; Liu, W.; Singh, H. Structure and Integrity of Liposomes Prepared from Milk- or Soybean-Derived Phospholipids during in Vitro Digestion. *Food Res. Int.* **2012**, *48*, 499–506.

(3) Théry, C.; Ostrowski, M.; Segura, E. Membrane Vesicles as Conveyors of Immune Responses. *Nat. Rev. Immunol.* **2009**, *9*, 581–593.

(4) van der Meel, R.; Fens, M. H.; Vader, P.; van Solinge, W. W.; Eniola-Adefeso, O.; Schiffelers, R. M. Extracellular Vesicles as Drug Delivery Systems: Lessons from the Liposome Field. *J. Controlled Release* **2014**, *195*, 72–85.

(5) Chapman, D. Phase Transitions and Fluidity Characteristics of Lipids and Cell Membranes. *Q. Rev. Biophys.* **1975**, *8*, 185–235.

(6) Lipowsky, R. Remodeling of Membrane Compartments: Some Consequences of Membrane Fluidity. *Biol. Chem.* **2014**, *395*.

(7) Neubauer, M. P.; Poehlmann, M.; Fery, A. Microcapsule Mechanics: From Stability to Function. *Adv. Colloid Interface Sci.* **2014**, *207*, 65–80.
(8) Sitterberg, J.; Özcetin, A.; Ehrhardt, C.; Bakowsky, U. Utilising Atomic Force Microscopy for the Characterisation of Nanoscale Drug Delivery Systems. *Eur. J. Pharm. Biopharm.* **2010**, *74*, 2–13.
(9) Briuglia, M.-L.; Rotella, C.; McFarlane, A.; Lamprou, D. A. Influence of Cholesterol on Liposome Stability and on in Vitro Drug Release. *Drug Deliv. Transl. Res.* **2015**, *5*, 231–242.
(10) Duangjit, S.; Pamornpathomkul, B.; Opanasopit, P.; Rojanarata, T.; Obata, Y.; Takayama, K.; Ngawhirunpat, T. Role of the Charge, Carbon Chain Length, and Content of Surfactant on the Skin Penetration of Meloxicam-Loaded Liposomes. *Int. J. Nanomedicine* **2014**, *9*, 2005.
(11) Maherani, B.; Arab-Tehrany, E.; Kheirolomoom, A.; Cleymand, F.; Linder, M. Influence of Lipid Composition on Physicochemical Properties of Nanoliposomes Encapsulating Natural Dipeptide Antioxidant L-Carnosine. *Food Chem.* **2012**, *134*, 632–640.
(12) Tokudome, Y.; Uchida, R.; Yokote, T.; Todo, H.; Hada, N.; Kon, T.; Yasuda, J.; Hayashi, H.; Hashimoto, F.; Sugibayashi, K. Effect of Topically Applied Sphingomyelin-Based Liposomes on the Ceramide Level in a Three-Dimensional Cultured Human Skin Model. *J. Liposome Res.* **2010**, *20*, 49–54.
(13) Yoshimoto, M.; Todaka, Y. Phase Transitioninduced Rapid Permeabilization of Liposome Membranes Composed of Milksphingomyelin. *Eur. J. Lipid Sci. Technol.* **2014**, *116*, 226–231.
(14) Inoue, K. Permeability Properties of Liposomes Prepared from Dipalmitoyllecithin, Dimyristoyllecithin, Egg Lecithin, Rat Liver Lecithin and Beef Brain Sphingomyelin. *Biochim. Biophys. Acta BBA-Biomembr.* **1974**, *339*, 390–402.
(15) Calò, A.; Reguera, D.; Oncins, G.; Persuy, M.-A.; Sanz, G.; Lobasso, S.; Corcelli, A.; Pajot-Augy, E.; Gomila, G. Force Measurements on Natural Membrane Nanovesicles Reveal a Composition-Independent, High Young's Modulus. *Nanoscale* **2014**, *6*, 2275–2285.
(16) Delorme, N.; Fery, A. Direct Method to Study Membrane Rigidity of Small Vesicles Based on Atomic Force Microscope Force Spectroscopy. *Phys. Rev. E* **2006**, *74*.
(17) Laney, D. E.; Garcia, R. A.; Parsons, S. M.; Hansma, H. G. Changes in the Elastic Properties of Cholinergic Synaptic Vesicles as Measured by Atomic Force Microscopy. *Biophys. J.* **1997**, *72*, 806.
(18) Li, S.; Eghiaian, F.; Sieben, C.; Herrmann, A.; Schaap, I. A. Bending and Puncturing the Influenza Lipid Envelope. *Biophys. J.* **2011**, *100*, 637–645.
(19) Liang, X.; Mao, G.; Simon Ng, K. . Probing Small Unilamellar EggPC Vesicles on Mica Surface by Atomic Force Microscopy. *Colloids Surf. B Biointerfaces* **2004**, *34*, 41–51.
(20) Ramachandran, S.; Quist, A. P.; Kumar, S.; Lal, R. Cisplatin Nanoliposomes for Cancer Therapy: AFM and Fluorescence Imaging of Cisplatin Encapsulation, Stability, Cellular Uptake, and Toxicity. *Langmuir* **2006**, *22*, 8156–8162.
(21) Liang, X.; Mao, G.; Ng, K. Y. S. Mechanical Properties and Stability Measurement of Cholesterol-Containing Liposome on Mica by Atomic Force Microscopy. *J. Colloid Interface Sci.* **2004**, *278*, 53–62.
(22) Benesch, M. G.; McElhaney, R. N. A Comparative Calorimetric Study of the Effects of Cholesterol and the Plant Sterols Campesterol and Brassicasterol on the Thermotropic Phase Behavior of Dipalmitoylphosphatidylcholine Bilayer Membranes. *Biochim. Biophys. Acta BBA-Biomembr.* **2014**, *1838*, 1941–1949.

(23) Redondo-Morata, L.; Giannotti, M. I.; Sanz, F. Influence of Cholesterol on the Phase Transition of Lipid Bilayers: A Temperature-Controlled Force Spectroscopy Study. *Langmuir* **2012**, *28*, 12851–12860.
(24) Garcia-Manyes, S.; Sanz, F. Nanomechanics of Lipid Bilayers by Force Spectroscopy with AFM: A Perspective. *Biochim. Biophys. Acta BBA - Biomembr.* **2010**, *1798*, 741–749.
(25) Picas, L.; Rico, F.; Scheuring, S. Direct Measurement of the Mechanical Properties of Lipid Phases in Supported Bilayers. *Biophys. J.* **2012**, *102*, L01–L03.
(26) Ahmed, S.; Nikolov, Z.; Wunder, S. L. Effect of Curvature on Nanoparticle Supported Lipid Bilayers Investigated by Raman Spectroscopy. *J. Phys. Chem. B* **2011**, *115*, 13181–13190.
(27) Marbella, L. E.; Yin, B.; Spence, M. M. Investigating the Order Parameters of Saturated Lipid Molecules under Various Curvature Conditions on Spherical Supported Lipid Bilayers. *J. Phys. Chem. B* **2015**, *119*, 4194–4202.
(28) Sorkin, R.; Dror, Y.; Kampf, N.; Klein, J. Mechanical Stability and Lubrication by Phosphatidylcholine Boundary Layers in the Vesicular and in the Extended Lamellar Phases. *Langmuir* **2014**, *30*, 5005–5014.
(29) Buchner Santos, E.; Morris, J. K.; Glynos, E.; Sboros, V.; Koutsos, V. Nanomechanical Properties of Phospholipid Microbubbles. *Langmuir* **2012**, *28*, 5753–5760.
(30) Prenner, E.; Chiu, M. Differential Scanning Calorimetry: An Invaluable Tool for a Detailed Thermodynamic Characterization of Macromolecules and Their Interactions. *J. Pharm. Bioallied Sci.* **2011**, *3*, 39.
(31) Bizien, T.; Ameline, J.-C.; Yager, K. G.; Marchi, V.; Artzner, F. Self-Organization of Quantum Rods Induced by Lipid Membrane Corrugations. *Langmuir* **2015**, *31*, 12148–12154.
(32) Blanton, T.; Barnes, C.; Lelental, M. Preparation of Silver Behenate Coatings to Provide Low-to Mid-Angle Diffraction Calibration. *J. Appl. Crystallogr.* **2000**, *33*, 172–173.
(33) Gaillard, C.; Douliez, J.-P. Cryo-TEM and AFM for the Characterization of Vesicle-like Nanoparticle Dispersions and Self-Assembled Supramolecular Fatty-Acid-Based Structures: A Few Examples. *Curr. Microsc. Contrib. Adv. Sci. Technol.* **2012**, *5*, 912–922.
(34) Murthy, A. V. R.; Guyomarc'h, F.; Lopez, C. Cholesterol Decreases the Size and the Mechanical Resistance to Rupture of Sphingomyelin Rich Domains, in Lipid Bilayers Studied as a Model of the Milk Fat Globule Membrane. *Langmuir* **2016**, *32*, 6757–6765.
(35) Fa, N.; Ronkart, S.; Schanck, A.; Deleu, M.; Gaigneaux, A.; Goormaghtigh, E.; Mingeot-Leclercq, M.-P. Effect of the Antibiotic Azithromycin on Thermotropic Behavior of DOPC or DPPC Bilayers. *Chem. Phys. Lipids* **2006**, *144*, 108–116.
(36) Fritzsching, K. J.; Kim, J.; Holland, G. P. Probing Lipid–cholesterol Interactions in DOPC/eSM/Chol and DOPC/DPPC/Chol Model Lipid Rafts with DSC and 13C Solid-State NMR. *Biochim. Biophys. Acta BBA - Biomembr.* **2013**, *1828*, 1889–1898.
(37) Grabielle-Madelmont, C.; Perron, R. Calorimetric Studies on Phospholipid—water Systems: I. Dl-Dipalmitoylphosphatidylcholine (DPPC)—water System. *J. Colloid Interface Sci.* **1983**, *95*, 471–482.
(38) Boni, L. T.; Minchey, S. R.; Perkins, W. R.; Ahl, P. L.; Slater, J. L.; Tate, M. W.; Gruner, S. M.; Janoff, A. S. Curvature Dependent Induction of the Interdigitated Gel Phase in DPPC Vesicles. *Biochim. Biophys. Acta BBA-Biomembr.* **1993**, *1146*, 247–257.

(39) Kuntsche, J.; Horst, J. C.; Bunjes, H. Cryogenic Transmission Electron Microscopy (Cryo-TEM) for Studying the Morphology of Colloidal Drug Delivery Systems. *Int. J. Pharm.* **2011**, *417*, 120–137.
(40) Colas, J.-C.; Shi, W.; Rao, V. M.; Omri, A.; Mozafari, M. R.; Singh, H. Microscopical Investigations of Nisin-Loaded Nanoliposomes Prepared by Mozafari Method and Their Bacterial Targeting. *Micron* **2007**, *38*, 841–847.
(41) Guyomarc'h, F.; Zou, S.; Chen, M.; Milhiet, P.-E.; Godefroy, C.; Vié, V.; Lopez, C. Milk Sphingomyelin Domains in Biomimetic Membranes and the Role of Cholesterol: Morphology and Nanomechanical Properties Investigated Using AFM and Force Spectroscopy. *Langmuir* **2014**, *30*, 6516–6524.
(42) Murthy, A. V. R.; Guyomarc'h, F.; Lopez, C. The Temperature-Dependent Physical State of Polar Lipids and Their Miscibility Impact the Topography and Mechanical Properties of Bilayer Models of the Milk Fat Globule Membrane. *Biochim. Biophys. Acta BBA - Biomembr.* **2016**, *1858*, 2181–2190.
(43) Leonenko, Z. V.; Finot, E.; Ma, H.; Dahms, T. E. S.; Cramb, D. T. Investigation of Temperature-Induced Phase Transitions in DOPC and DPPC Phospholipid Bilayers Using Temperature-Controlled Scanning Force Microscopy. *Biophys. J.* **2004**, *86*, 3783–3793.
(44) Nagle, J. F.; Tristram-Nagle, S. Structure of Lipid Bilayers. *Biochim. Biophys. Acta BBA-Rev. Biomembr.* **2000**, *1469*, 159–195.
(45) Rawicz, W.; Olbrich, K.; McIntosh, T.; Needham, D.; Evans, E. Effect of Chain Length and Unsaturation on Elasticity of Lipid Bilayers. *Biophys. J.* **2000**, *79*, 328–339.
(46) Garcia-Manyes, S.; Oncins, G.; Sanz, F. Effect of Temperature on the Nanomechanics of Lipid Bilayers Studied by Force Spectroscopy. *Biophys. J.* **2005**, *89*, 4261–4274.
(47) Redondo-Morata, L.; Oncins, G.; Sanz, F. Force Spectroscopy Reveals the Effect of Different Ions in the Nanomechanical Behavior of Phospholipid Model Membranes: The Case of Potassium Cation. *Biophys. J.* **2012**, *102*, 66–74.
(48) Jacquot, A.; Francius, G.; Razafitianamaharavo, A.; Dehghani, F.; Tamayol, A.; Linder, M.; Arab-Tehrany, E. Morphological and Physical Analysis of Natural Phospholipids-Based Biomembranes. *PLoS ONE* **2014**, *9*, e107435.
(49) Reissner, E. Note on the Membrane Theory of Shell of Revolution. *Stud. Appl. Math.* **1947**, *26*, 290–293.
(50) Fery, A.; Weinkamer, R. Mechanical Properties of Micro- and Nanocapsules: Single-Capsule Measurements. *Polymer* **2007**, *48*, 7221–7235.
(51) Glaubitz, M.; Medvedev, N.; Pussak, D.; Hartmann, L.; Schmidt, S.; Helm, C. A.; Delcea, M. A Novel Contact Model for AFM Indentation Experiments on Soft Spherical Cell-like Particles. *Soft Matter* **2014**, *10*, 6732.
(52) Berry, J. D.; Mettu, S.; Dagastine, R. R. Precise Measurements of Capsule Mechanical Properties Using Indentation. *Soft Matter* **2017**, *13*, 1943–1947.
(53) Makino, K.; Yamada, T.; Kimura, M.; Oka, T.; Ohshima, H.; Kondo, T. Temperature- and Ionic Strength-Induced Conformational Changes in the Lipid Head Group Region of Liposomes as Suggested by Zeta Potential Data. *Biophys. Chem.* **1991**, *41*, 175–183.
(54) Meleard, P.; Gerbeaud, C.; Pott, T.; Fernandez-Puente, L.; Bivas, I.; Mitov, M. D.; Dufourcq, J.; Bothorel, P. Bending Elasticities of Model Membranes: Influences of Temperature and Sterol Content. *Biophys. J.* **1997**, *72*, 2616.
(55) Duwe, H. de; Sackmann, E. Bending Elasticity and Thermal Excitations of Lipid Bilayer Vesicles: Modulation by Solutes. *Phys. Stat. Mech. Its Appl.* **1990**, *163*, 410–428.

(56) Hantz, E.; Cao, A.; Escaig, J.; Taillandier, E. The Osmotic Response of Large Unilamellar Vesicles Studied by Quasielastic Light Scattering. *Biochim. Biophys. Acta BBA-Biomembr.* **1986**, *862*, 379–386.
(57) Brochu, H.; Vermette, P. Young's Moduli of Surface-Bound Liposomes by Atomic Force Microscopy Force Measurements. *Langmuir* **2008**, *24*, 2009–2014.
(58) Dieluweit, S.; Csiszár, A.; Rubner, W.; Fleischhauer, J.; Houben, S.; Merkel, R. Mechanical Properties of Bare and Protein-Coated Giant Unilamellar Phospholipid Vesicles. A Comparative Study of Micropipet Aspiration and Atomic Force Microscopy. *Langmuir* **2010**, *26*, 11041–11049.
(59) Dimitriadis, E. K.; Horkay, F.; Maresca, J.; Kachar, B.; Chadwick, R. S. Determination of Elastic Moduli of Thin Layers of Soft Material Using the Atomic Force Microscope. *Biophys. J.* **2002**, *82*, 2798–2810.
(60) Shull, K. R. Contact Mechanics and the Adhesion of Soft Solids. *Mater. Sci. Eng. R Rep.* **2002**, *36*, 1–45.
(61) Sullan, R. M. A.; Li, J. K.; Zou, S. Direct Correlation of Structures and Nanomechanical Properties of Multicomponent Lipid Bilayers. *Langmuir* **2009**, *25* , 7471–7477.
(62) Li, J. K.; Sullan, R. M. A.; Zou, S. Atomic Force Microscopy Force Mapping in the Study of Supported Lipid Bilayers. *Langmuir* **2011**, *27*, 1308–1313.
(63) Marsh, D. Elastic Curvature Constants of Lipid Monolayers and Bilayers. *Chem. Phys. Lipids* **2006**, *144*, 146–159.
(64) Niggemann, G.; Kummrow, M.; Helfrich, W. The Bending Rigidity of Phosphatidylcholine Bilayers: Dependences on Experimental Method, Sample Cell Sealing and Temperature. *J. Phys. II* **1995**, *5*, 413–425.
(65) Boggs, J. M. Intermolecular Hydrogen Bonding between Lipids: Influence on Organization and Function of Lipids in Membranes. *Can. J. Biochem.* **1980**, *58*, 755–770.
(66) Slotte, J. P. The Importance of Hydrogen Bonding in Sphingomyelin's Membrane Interactions with Co-Lipids. *Biochim. Biophys. Acta BBA-Biomembr.* **2016**, *1858*, 304–310.
(67) Chen, Q.; Vancso, G. J. pH Dependent Elasticity of Polystyrene-Block-Poly(acrylic Acid) Vesicle Shell Membranes by Atomic Force Microscopy. *Macromol. Rapid Commun.* **2011**, *32*, 1704–1709.

TABLES

Table1: Geometrical parameters of dioleoylphosphatidylcholine (DOPC) or dipalmitoylphosphatidylcholine (DPPC) liposomes and their corresponding membrane thicknesses. The height (*H*) and width (*W*) mean values were measured using the cross section of AFM images of the liposomes and used to calculate the volume of the adsorbed liposomes,

from which the mean diameter of a sphere of equivalent volume was deduced (Eq.2). The mean values of DOPC and DPPC membrane thicknesses were measured using the jump distance d from breakthrough force curves (n=30) recorded in PIPES/NaCl/$CaCl_2$ buffer, pH 6.7 at 20°C.

Lipid	Mean height H of liposomes by AFM (nm)	Mean width W of liposomes by AFM (nm)	Mean diameter of equivalent sphere by AFM (nm)	Mean diameter of liposomes by DLS (nm)	Membrane thickness by AFM (nm)
DOPC	**59 ± 27**	**310 ± 97**	**150 ± 90**	**120 ± 69**	**3.91 ± 0.41**
DPPC	**151±48**	**448 ± 154**	**296 ± 88**	**132 ±73**	**4.93 ± 0.47**

Table 2: Comparison of the bending modulus (k_C) and Young modulus values (E) of liposomes or of supported lipid bilayers in the fluid or gel phase reported in the literature using different techniques as indicated. Abbreviations stand for: EggPC = mixture of unsaturated (54.8 wt. %) and saturated (45.2 wt. %) phosphatidylcholine; DMPC = 1,2-dimyristoyl-sn-glycero-3-phosphocholine; ESM = egg sphingomyelin; Chol = cholesterol. Values in italics were calculated by the authors using calculations described in the Appendix (eq.A.2; A.3)

684

Reference	Lipid	Technique	Phase	Bending modulus k_C ($\times 10^{-19}$J)	Young modulus E (MPa)
		Liposomes (3D)			
Present work	DOPC	AFM spectroscopy	Fluid	0.9	13
	DPPC	AFM spectroscopy	Gel	15.50	116
16	DPPC	AFM spectroscopy	Gel	*13.54*	110
21	Egg PC	AFM spectroscopy	Fluid	0.27	1.97
45	synthetic phospholipids (18:1)	Micropipette pressurization	Fluid	0.90	*12.70*
54	DMPC	Phase contrast microscopy	Fluid	1.27	*26*
55	DMPC	Phase contrast microscopy	Fluid	1.15	*24*
56	DOPC	Osmotic swelling	Fluid	*1.06*	15
		Supported bilayers (2D)			
Present work	DOPC	AFM spectroscopy	Fluid	0.88	27
	DPPC	AFM spectroscopy	Gel	2.03	31
28	DOPC	AFM spectroscopy	Fluid	1.69	19.3
	DPPC	AFM spectroscopy	Gel	2.33	28.1
61	DOPC	AFM spectroscopy	Fluid	*4.61*	80
	ESM/Chol	AFM spectroscopy	Liquid ordered	*12.94*	140
62	DOPC	AFM spectroscopy	Fluid	*8.65*	150
	ESM/Chol	AFM spectroscopy	Liquid ordered	*27.72*	300

685

686

687

688

689

690

691

692

693

FIGURES:

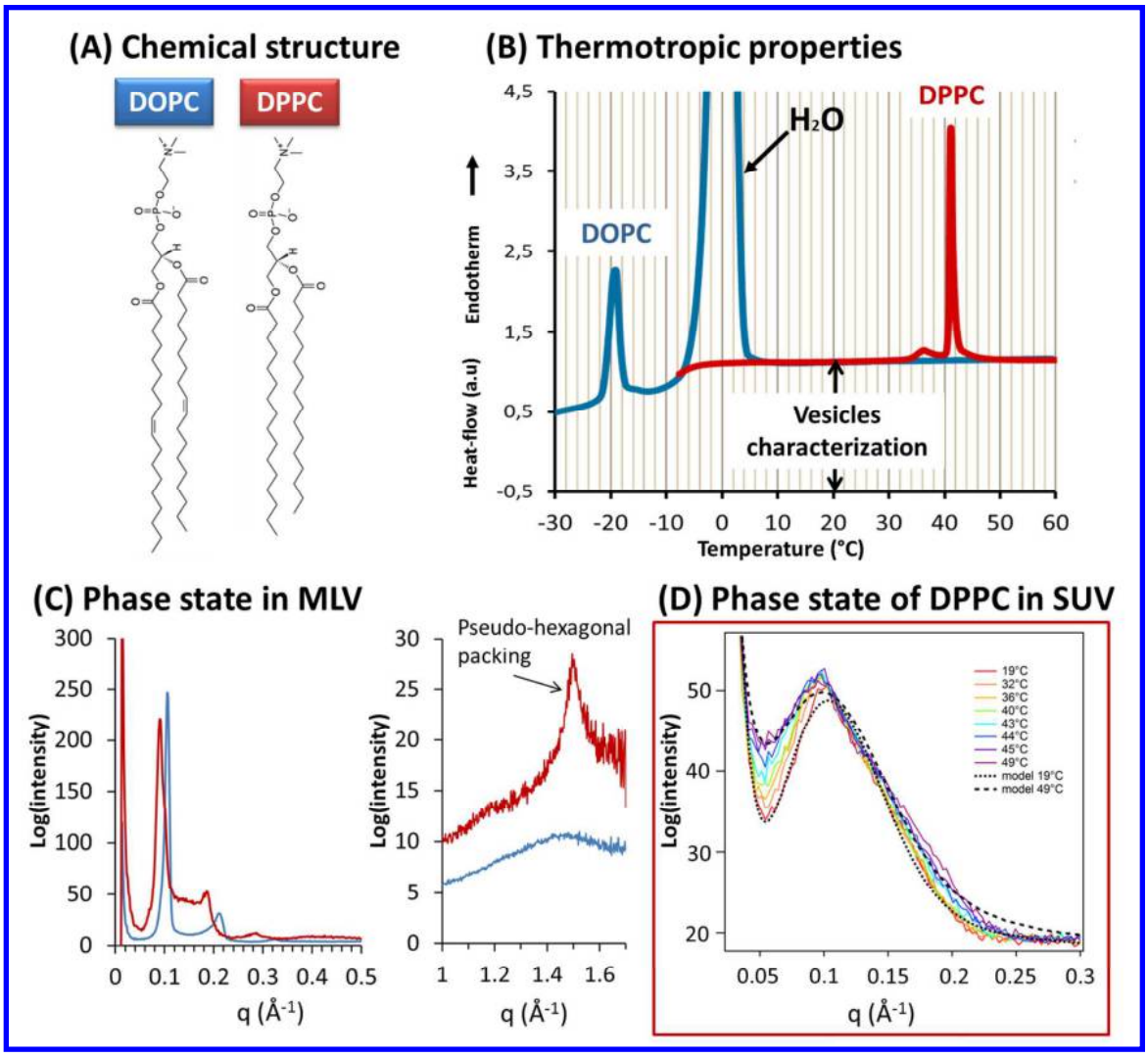

Figure 1: (A) Molecular structures of the unsaturated DOPC (dioleoylphosphatidylcholine) and saturated DPPC (dipalmitoylphosphatidylcholine). (B) Differential scanning calorimetry thermograms of DOPC (blue trace) and DPPC (red trace) multilamellar vesicles recorded on heating at 2°C.min^{-1}. (C) X-ray diffraction patterns of DOPC and DPPC fully hydrated multilamellar vesicles recorded at 20°C at small (left) and wide (right) angles. (D) Small angle X-ray Scattering of DPPC SUV recorded on heating. Unilamellar SAXS model at low

and high temperature are superimposed. All experiments were performed in aqueous PIPES/NaCl/$CaCl_2$ medium at pH = 6.7.

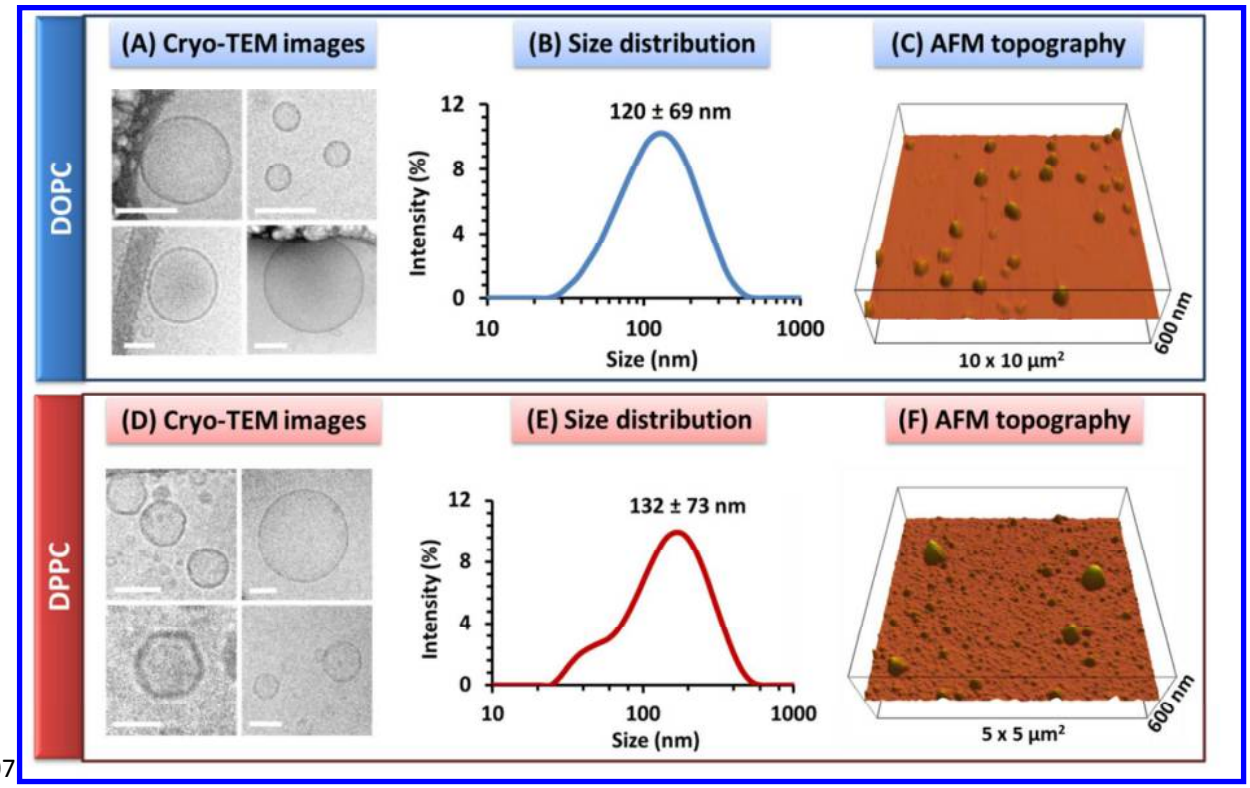

Figure2: Characterization of the shape and size of DOPC (dioleoylphosphatidylcholine) or DPPC (dipalmitoylphosphatidylcholine) liposomes. (A) and (D) Cryo-TEM images of the DOPC and DPPC liposomes, respectively; scale bars are 100 nm. (B) and (E) Dynamic light scattering size distribution in intensity of the DOPC and DPPC liposome suspensions, respectively; and (C) and (F) typical AFM 3D images of DOPC and DPPC liposomes, respectively. All experiments were performed in aqueous PIPES/NaCl/$CaCl_2$ medium at pH = 6.7 and at 20°C.

716

717

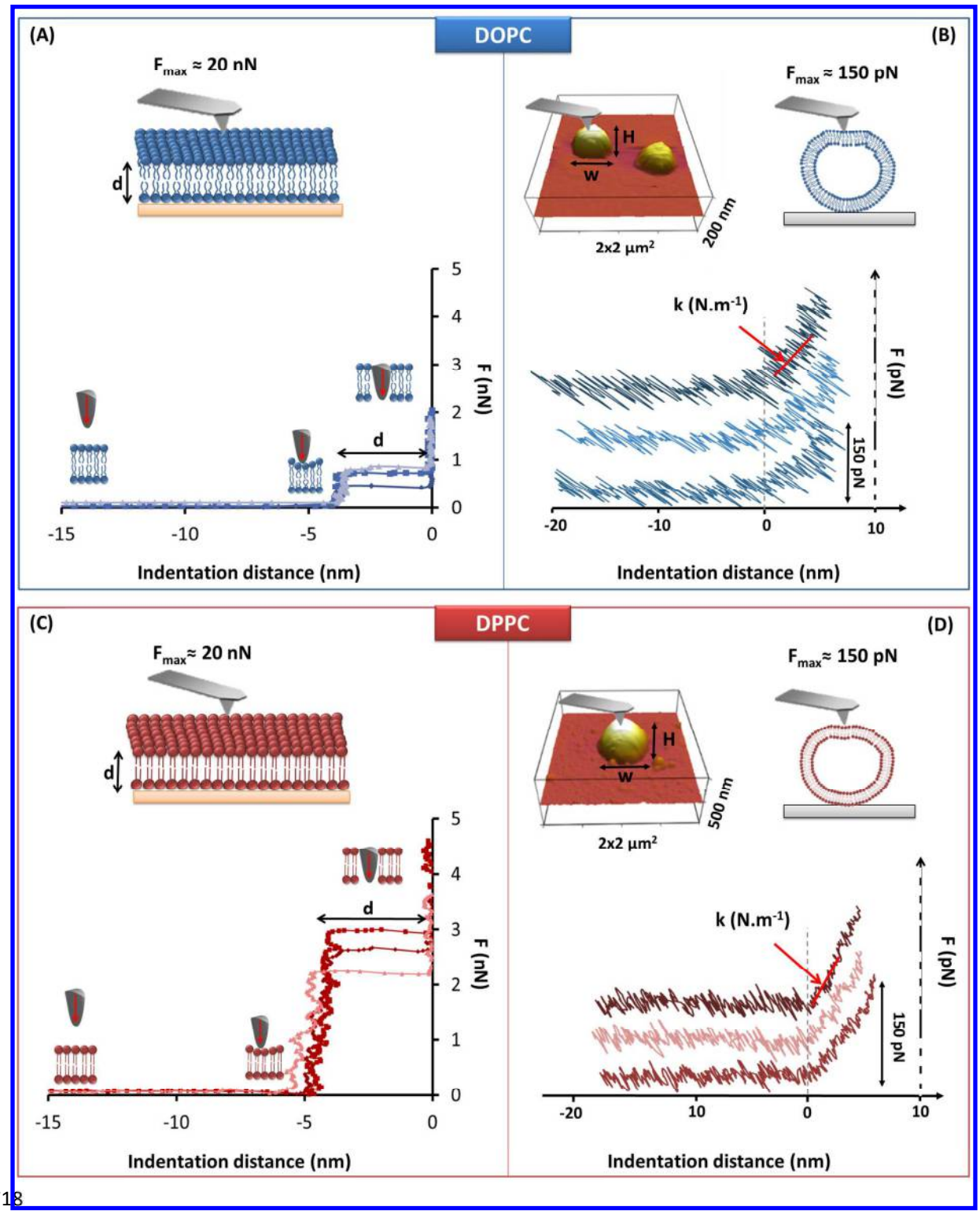
(A)
DOPC
(B)
F_{max} ≈ 20 nN
d
H
w
200 nm
2x2 µm²
F_{max} ≈ 150 pN
k (N.m⁻¹)
F (pN)
150 pN
F (nN)
Indentation distance (nm)
Indentation distance (nm)
(C)
DPPC
(D)
F_{max}≈ 20 nN
F_{max}≈ 150 pN
500 nm
2x2 µm²
k (N.m⁻¹)
F (pN)
150 pN
F (nN)
Indentation distance (nm)
Indentation distance (nm)

718

Figure 3: AFM indentation measurement on DOPC (dioleoylphosphatidylcholine, in blue) or DPPC (dipalmitoylphosphatidylcholine, in red) liposomes adsorbed on silicon substrate. (A) and (C) show the breakthrough force curves obtained as a result of tip penetration into DOPC or DPPC supported lipid bilayers, respectively. The average bilayer thickness value d was measured from the jump-through distance (n=50). (B) and (D) show typical force curves acquired during indentation of, respectively, DOPC or DPPC liposomes in the elastic regime; in order to infer the bilayer stiffness *k* from the slope after tip-membrane contact. For the sake of clarity, the force curves are shifted along the Y axis. All measurements were recorded in aqueous PIPES/NaCl/$CaCl_2$ medium at pH = 6.7 and at 20°C.

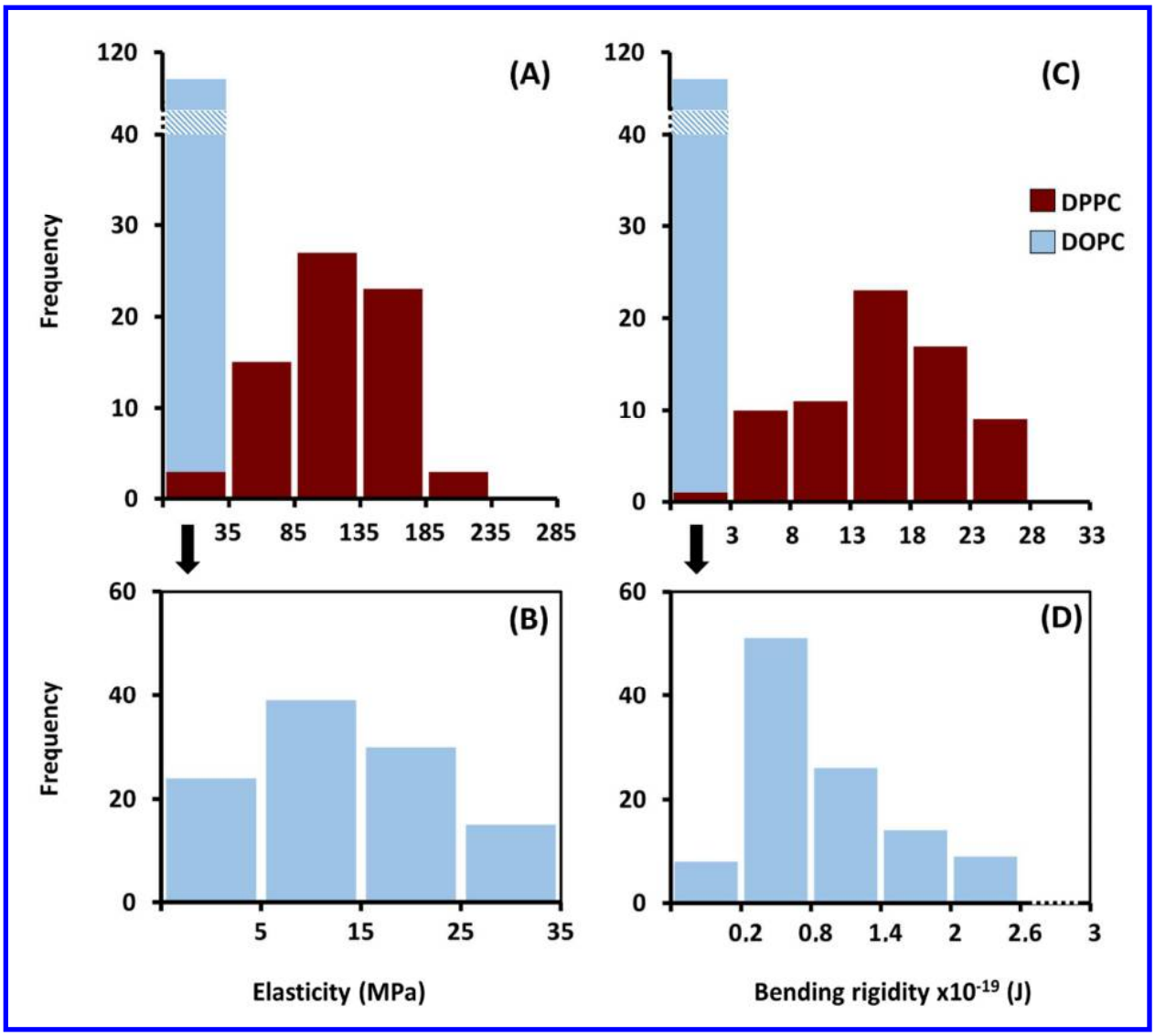

Figure 4: Distributions of the Young moduli E and of the bending rigidity k_C, independent of liposome size, of DOPC (n=108) and DPPC (n=71). (A) and (C) show the superposition of both DOPC and DPPC frequency distributions for E and k_C, respectively. (B) and (D) show

respective enlargements of the E and k_C frequency distributions for the DOPC liposomes. All measurements were recorded in aqueous PIPES/NaCl/$CaCl_2$ medium at pH = 6.7 and at 20°C.

Table of contents graphic